A Yellow–Orange Wavelength-Based Short-Term Heart Rate Variability Measurement Scheme for Wrist-Based Wearables

Payal Mohapatra, Preejith Sreeletha Premkumar, and Mohanasankar Sivaprakasam

***Abstract*— Heart rate variability (HRV) is one of the important biomarkers of physical and psychological well-being. Hence, a convenient and minimally intrusive method for HRV measurement is advantageous. Although high levels of surrogacy of short-term HRV estimates obtained from the measurements of blood volume changes to traditional electrocardiographic (ECG) measurements have been reported, no detailed account on extraction of such parameters from a wrist-based optical monitor is found in the literature. In this paper, a yellow–orange wavelength-based optical scheme is incorporated into a wearable device for HRV estimation from dorsal side of the wrist. This design is pivotal in catering to a wider span of population with varied skin tones. The developed wearable in alliance with a gateway device is capable of picking up photoplethysmography from the measurement site, allowing estimation of HRV-indices within a confidence of 5% from ECG-derived parameters. The HRV measurement ecosystem is validated under the setting of three postural loads for 20 subjects, generating 60 data sets. Study results show statistically significant positive correlation and nonsignificant bias in Bland–Altman analysis, for the HRV-indices derived from either method. In most of the extracted HRV features, the observations in supine position showed minimum deviation from the reference. Estimation of short-term HRV-indices from wrist-based photoplethysmography under stationary conditions shows promising results from the study. Electrical and biological noninterference and ease of usage of the proposed design simplify stationary and ambulatory monitoring of HRV.**

***Index Terms*— Heart rate variability (HRV), orthostatic stress, personal health monitors, photoplethysmography, postural loads, wearables, wrist-based photoplethysmogram.**

I. Introduction

WITH changes in the requirement of body, autonomic output regulates cardiac functionality to ensure and maintain internal stasis. A human heart does not have fixed interbeat period and this variation in subsequent cardiac cycles captured over a period is called heart rate variability (HRV). Any ectopic beats or irregular heartbeats cannot be used for HRV computation. Hence, normal-to-normal interval (NN-interval) is used to denote the series of intercardiac cycle durations [1]. Measures of HRV can provide noninvasive information on vagal and sympathetic components of the autonomic nervous system (ANS) and can be used as a physiological marker for many pathological conditions. A decrease in HRV is associated with the risk of many cardiac events [2]–[5]. Recent developments have shown the contribution of HRV to index cardiac vagal tone, which is relevant for many psychophysiological studies, including self-regulation at cognitive, social, and emotional levels [6], [7]. Also, the power spectra of NN-interval series have been found to relate to the autonomic cardiovascular control [8]. HRV is a significant marker to assess the training, performance, and endurance levels in athletes [9]. Additionally, depression and other psychological abnormalities affect the ANS and hence, the HRV [10]. The extent of variability is traditionally obtained by digitally processing electrocardiographic (ECG) signal. The distinct profile of R-peaks in ECG makes it suitable to be programmatically detected. Hence, the standard method to assess the cardiac cycles is to place their bounds at the R-peaks. Various temporal and spectral features of these intervals form the array of HRV indices used for measurement [11]. Measurement of 24-h ECG is not feasible for widespread epidemiological studies and may also be unnecessary. Bigger *et al.* [12] have shown a correlation greater than 0.75 between a 2–15 min and a 24-h HRV measurement post MI on 715 subjects for mortality predictors and sudden cardiac death. Studies have shown that short-term HRV is stable and applicable in the assessment of overall psychic and somatic fitness [13].

Optical photoplethysmography manifests the activity of the heart by assessing blood volume change and evaluating peripheral circulation [14]. Owing to simplicity in operation, wide applicability in clinical routine, and increasing incorporation in wearable health monitoring devices [14], it is desirable to explore additional measurements from photoplethysmography (PPG). Studies have shown the surrogacy of HRV derived from the variation of successive pulse durations in PPG [referred as pulse rate variability (PRV)] to the HRV derived from the gold-standard ECG [15]. Most of such studies utilize only the extremities of the body as the measurement site of PPG such as finger [16] and earlobes [17]. Schäfer and Vagedes have extensively compared the various techniques used to derive PRV, and consolidated the findings to the measurement sites, like various fingers, earlobes, and forehead [18]. In the available literature, justified reports stating the usability of wrist-based reflective PPG technique

Manuscript received July 2, 2017; revised September 3, 2017; accepted October 23, 2017. The Associate Editor coordinating the review process was Dr. Vedran Bilas. *(Corresponding author: Payal Mohapatra.)*

P. Mohapatra is with the Department of Electrical Engineering, IIT Madras, Chennai 600036, India (e-mail: ee15s049@ee.iitm.ac.in).

P. S. Premkumar is with the Healthcare Technology Innovation Center, IIT Madras, Chennai 600113, India.

M. Sivaprakasam is with the Department of Electrical Engineering, IIT Madras, Chennai 600036, India, and also with the Healthcare Technology Innovation Center, IIT Madras, Chennai 600113, India.

Color versions of one or more of the figures in this paper are available online at http://ieeexplore.ieee.org.

Digital Object Identifier 10.1109/TIM.2017.2786677

in deriving PRV are not prominent. However, very limited works [19] have employed the dorsal side of the wrist as a measurement site with a sampling rate of 20 Hz (or less), but a recent study [20] indicates the ideal choice of sampling rate for accurate detection of HRV indices from PPG to be a minimum of 25 Hz. Another study employing the Polar S810 to estimate PRV accurately has analyzed the time-domain indices in two postures. The results show high degree of agreement with ECG as reference, using various statistical methods. However, the validity of frequency-domain indices and the sampling rate used were not found to be reported [21]. The wrist-based reflective PPG technique has wide potential in measuring physiological parameters, like the oxygen saturation level [22], respiratory activity [23], and cuffless blood pressure [24] apart from heart rate. Developing technology to reliably extract NN-intervals and hence, HRV from such wearable devices would further enhance their use. A number of people need daily monitoring of HRV, as a predictor of their stress levels, improvement in physical fitness, and so on apart from cardiac and ANS specific ailments. Enabling a reliable measurement of short-term HRV from a wrist-based wearable furthers the progression to individual-centered healthcare with almost negligible hindrance to the regular lifestyle. This unobtrusive and nonrestraining nature of a wristwatch form factor wearable motivated us to develop a comprehensive device. This allows the measurement of short-term HRV under stationary conditions by considering appropriate hardware and sampling rate requirements.

Mathias and Bannister [25] have shown changes in autonomic cardiovascular function in response to various orthostatic stressors and their use in estimating the health of ANS, wherein the relation between symptoms and postural change is the key component [26]. Different postures are used during HRV measurement, as diagnosis varies under various postural stimuli [27]. Supine position renders parasympathetic saturation whereas, a standing posture causes sympathovagal imbalance. Since a consistent choice of position during HRV measurement is a prime element, it is important to study the validity of PRV under various postural loads.

In this paper, we present a system to derive prominent time- and frequency-domain features of short-term HRV using a novel yellow–orange (590 nm) wavelength scheme, which is relatively insensitive to melanin for optical sensing in a wrist-based wearable. The design details and specifics involved in the proposed measurement technique are elaborated in Section II. The selection of optical elements, sensor topology and fabrication of the optical sensor board and the hardware involved in the front end are described in Sections II-A and II-B, respectively. An adaptive thresholding technique is established and implemented for reliable and repeatable interbeat detection, as detailed in Section II-C. The pronounced effect of ANS due to different body postures [28] and corresponding changes in HRV are experimentally validated in an *in vivo* study on 20 subjects in three different postures. The study conducted using the developed PPG sensor to extract pulse-derived HRV is compared with HRV obtained using a standard ECG setup. *In vivo* validation, study objective, and experimental protocol are described in Section III. Experimental results of a pilot study conducted on six pigmented male subjects to verify the advantage of 590-nm optical scheme in alignment with the results reported in the previous work of the authors [29] are given in Section IV-A. Detailed statistics and analysis of the measured HRV parameters are discussed in Section IV-B. Finally, Section V summarizes and concludes this paper.

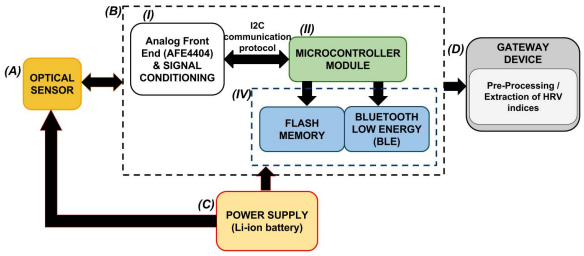

Fig. 1. System level architecture. The modules are labeled as (A) optical sensor unit, (B) mother board consisting of (I) system hardware (analog front end and signal conditioning circuit, digital accelerometer), (II) microcontroller unit, and (III) data storage and streaming unit, (C) power unit, and (D) gateway device (tablet/personal computer/smartphone).

II. Measurement Methodology

A wrist-based optical wearable is designed using the technique of reflective photoplethysmography, to work in conjunction with a host processor. A yellow–orange (590 nm) wavelength optical sensor topology is used, which is relatively insensitive to skin pigmentation levels [29]. Further details supporting this choice are given in Section II-A. The motherboard houses an analog front end, AFE4404, by Texas Instruments, a microcontroller unit to program the basic functionalities and communication between the modules, and a data streaming and storage unit for off-line data analysis. The modular level break down is shown in the system architecture in Fig. 1 with detailed annotations. This system is capable of measuring HRV indices (time and frequency) with a high degree of confidence ($\alpha < 5\%$). The algorithms for preprocessing and extraction of HRV indices are employed in the host processor for either off-line or real-time analysis, as required.

A. Optical Sensor Design

In reflective PPG, optical emitter unit is used to shine light onto the measurement site, whose properties are modulated by the direct pulsation in arteries or palpated through the capillaries. This pulsatile quasi-periodic optical signal is received by a photodetector. The bones, tendons, muscles, fat, and so on introduce an additional time-invariant component to the acquired signal. Quality of signal picked up by the sensor largely depends on the optical properties of skin as well. Anderson and Parrish [30] have reported an absorption window of 350–1200 nm for melanin. Such a dermal property hinders the strength of signal picked up by the photodetector for pigmented subjects. From Fig. 2, a decrease in the absorption coefficient of melanin with progressing wavelength

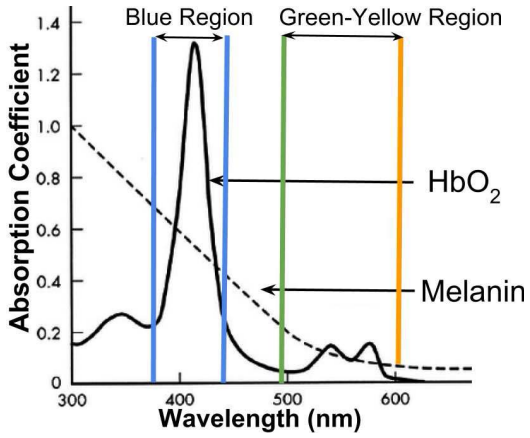

Fig. 2. Relation between melanin and HbO_2 absorption coefficient and wavelength [30]. There is a progressive decrease in melanin absorption coefficient with increase in wavelength. Hence, the choice of wavelength with escalated HbO_2 absorption is made toward the secondary peak ranging between 500 and 600 nm to have relatively less sensitivity to melanin.

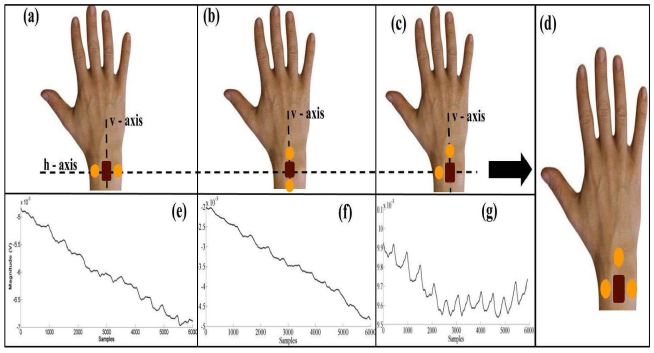

Fig. 3. Experimentation with different optical topologies. (a) and (b) LEDs placed at 180° with respect to each other. (c) LEDs placed at 90° with respect to each other with the vertex at the PD. (d) Final topology with a symmetrically opposite LED along the *h*-axis to provide redundancy in case of loss of contact in the event of tilt or improper placement by wrist bone. (e) and (f) Waveforms corresponding to configurations shown in (a)–(c), respectively.

can be seen. Since water absorbs light with wavelength greater than 1000 nm [31], wavelengths beyond 1000 nm are not suitable as optical emitters. Superiority of shorter wavelengths like green over infrared (IR) has been shown in the literature [32], [33]. IR light has a high optical penetration depth [34]. This makes IR extremely susceptible to even mild movements, hence, less suitable for wrist-based wearables. Thus, the identification of suitable wavelength for the current optical emitter was conducted in the visible spectrum. From Fig. 2, it can be observed that the dominant peak of the HbO_2 absorption coefficient is in the blue region, followed by the yellow–green region. Since melanin absorption coefficient is high in the blue region, the signal quality was found to be poor. Further tests were conducted in the green–yellow region between 500 and 600 nm to identify the wavelength which provides the strongest signal corresponding to pulsatile blood flow. Experiments were conducted on numerous LEDs with wavelengths in the range of 500–600 nm subject to their commercial availability, and the results attained with 590-nm (yellow–orange) wavelength were the most favorable. This is a justified choice, as toward the later end of the span of chosen visible spectra, there is prominently high absorption coefficient for HbO_2 and relatively lower absorption corresponding to melanin. A study on the response of 590-nm wavelength as compared with the traditional choice of green (500–540 nm) wavelength on varied skin-tone subjects is presented, and affirmative results on the relative insensitivity of 590-nm optical scheme to melanin are reported in the previous work of the authors [29]. Such a choice allows to expand the utility of the wearable to subjects with varied skin pigmentation levels.

The proposed design for optical sensor configuration has two fundamental units: emitter and detector. A wideband photodiode (PD) (TEMD5080X01) with an exposed area of reception of 70 mm^2 and a comparable spectral response over the entire visible region is used as the detector in the design. Black package dome lens (beam angle of 30°) light-emitting diodes (LEDs) are used as the optical emitters. The 30° beam angle ensures enhanced focus and intensity. The black package reduces reflections caused by incident light or any other light bleeding issues. A 590-nm (yellow–orange) LED (LYT64F) is used in the design. Different configurations of optical arrangement, as shown in Fig. 3(a)–(c), were experimentally tested. Representative PPG waveforms collected from a subject consecutively for the illustrated topologies in Fig. 3(a)–(c) at a sampling rate of 500 Hz are shown in Fig. 3(e)–(g), respectively. The arrangement of LEDs at 90° with respect to each other, with PD as vertex as shown in Fig. 3(c), showed preferential results over the LEDs arranged at 180° with respect to each other, as shown in Fig. 3(a) and (b). Adopting the configuration shown in Fig. 3(c), a symmetrically opposite LED is placed along the horizontal (h) axis, as shown in Fig. 3(d), to ensure a definitive contact in case of tilted motion or improper placement due to wrist bone. The configuration is aimed to maximize the area of illumination, and the LEDs are positioned in a "*T*"-profile on the sensor board with the PD on the junction of the h-axis, which harbors two symmetrically positioned LEDs (LED 1 and LED 2) and the vertical (v) axis containing LED 3, as shown in Fig. 4(a). A custom designed PCB with sufficiently long solder pads was initially used to arrive upon the optimum separation between the optical elements. This was done to ensure negligible direct optical coupling that may saturate the signal acquired by the photodetector and allow maximum admission of the reflected light containing PPG information. The PD and LEDs are aligned to the same transverse plane for escalated light admission and reception. To avoid any instance of direct coupling, appropriate optical isolators house the emitter and detector units.

In the previously developed experimental prototype presented in [29], black silicon blocks were filed and aligned adeptly to achieve the optical isolation. In the current design, individual housings for each optical component are prototyped on the back side of the enclosure. The cavities are meticulously carved out to allow a perfect fit when the enclosure sits on the sensor board. In the previous design using a wired prototype presented in [29], an H-bridge configuration for LED driver circuit was used. Since the front end used in this device

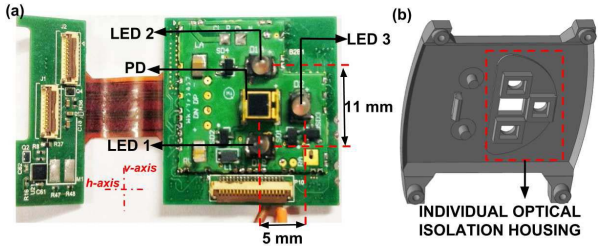

Fig. 4. (a) Optical sensor PCB illustrates the elements, which are annotated as per their reference in the design. The dimensions for optimal separation are also indicated along with the h-axis and v-axis. (b) Back end of the enclosure casing, which provides meticulously carved out cavities for the optical elements to provide absolute isolation within the components.

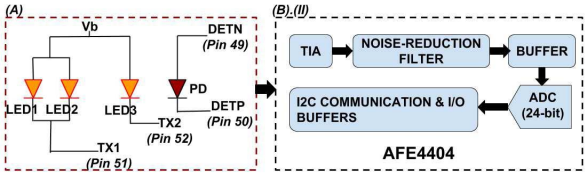

Fig. 5. Common-anode connection for the optical emitter scheme. LED1 and LED2 are parallelly connected to the first channel and LED3 is connected to the second channel. The PD is connected to the front end for signal admission. The respective pins where connections are made are also annotated in the illustration. (A) Optical sensor unit. (B) Analog front end.

supports only a push–pull configuration, the sensor board uses a common-anode mode for driving the LEDs, as shown in Fig. 5. The annotations in Fig. 5 map to the system architecture shown in Fig. 1. Also, Fig. 5 indicates the respective pin numbers of the front end (AFE4404, as explained later) to which the connections are made. LED 1 and LED 2 are connected in parallel to the same driving channel of the front end and LED 3 is driven by a separate channel. To improve the practicality of the device, a direct contact of the optical components to skin is not allowed, and least any external factors like sweat, moisture, and so on affect the optical coupling. A poly methyl methacrylate (PMMA) glass is placed between the skin and the optical elements. The absorption spectra of PMMA blends have shown minimal absorption coefficients in the visible spectra [35], and hence, this incorporation does not deteriorate the signal quality of the PPG waveform. The exploded view of the entire design shown in Fig. 6 indicates the partitioned PMMA glass slices for the respective optical elements. The backside of the enclosure exposed to the dermal surface is engraved depthwise to enable the accommodation of this glass covering on the same plane without any additional projection or increase in the width.

B. Hardware Requirements of the Device and Data Acquisition

An analog front end provided by Texas Instruments, AFE4404, is used in the design. The previous wired prototype [29] used AFE4403 as the analog front end. The current choice of AFE4404 is made to achieve an improved ADC resolution of 24 bits as compared with the 22 bits. The AFE4404 communicates with the microcontroller using an I2C communication protocol. The front end can provide

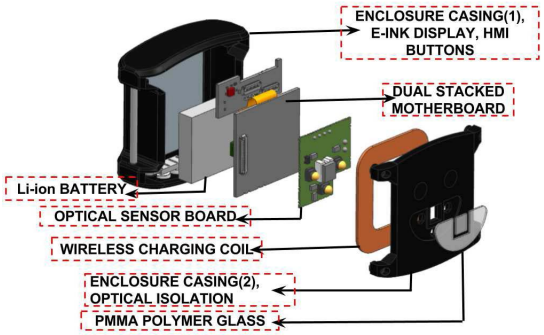

Fig. 6. Exploded view of the device showing the arrangement of all the modules.

both a raw captured signal and an ambient signal. However, to economically sustain the power usage, only ambient subtracted raw waveform sampled at 500 Hz is stored/streamed. The gain of the transimpedance amplifier can be adjusted by manipulating the dedicated registers. AFE4404 is available in a DSBGA package of 2.6 mm $\times$ 1.6 mm. The basic modules of AFE4404 are highlighted in Fig. 5(B)-(II). An MEMs' 3-axis accelerometer from Analog Devices Inc., (ADXL333) is integrated along with, to allow identification of stationary sections of the recorded data. Other suitable techniques, like adaptive template matching scheme provided by Orphanidou *et al.* [36], may also be used to segregate the stationary sections, in case additional accelerometer hardware is unavailable. A low-power consuming Bluetooth low energy (BLE) module of small form-factor is used in the design to stream data in real-time data for online analysis or store in a gateway device for off-line processing and analysis. The prototype is also provided with on-chip flash drive. The device is powered by a rechargeable 200-mAh Li-ion battery and can be charged wirelessly using any compatible wireless charger commercially available. Both the PCB and the enclosure design are achieved using Altium design suit and Siemens NX CAD software, respectively. The teardown of the device is shown in Fig. 6. Additionally, to allow hassle-free interaction, some peripheral features, like e-ink display and two push buttons on the side of the device, are provided. The gateway device is featured similar to a tablet for this prototype; however, it can be replaced by any personal computer or smartphone. The platform for waveform acquisition and off-line logging is developed using LabVIEW 2015. Fig. 7(a) shows the optical sensor board with wireless charging coil. Fig. 7(b) shows the backside of the wearable which is in dermal contact. Fig. 7(c) shows a overall measurement system with the wearable placed on the dorsal side of the nondominant hand of the subject along with a gateway device. For the standard reference, ECG signal was acquired using eMotion Faros 360° (Mega Electronics) in single lead configuration sampled at a rate of 1000 Hz. The collected ECG and PPG signals are appropriately time synchronized prior to any processing.

C. Analytical Methods

Use of PPG to derive the HRV is denoted as PRV and the terminology HRV will resort to the variability obtained

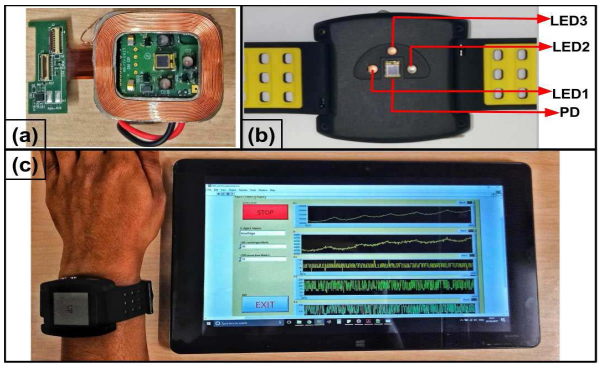

Fig. 7. (a) Designed optical sensor unit and wireless charging coil. (b) Back side of the wearable exposed to the dermal area indicating the placement and topology of the optical elements. (c) Wrist-based wearable to estimate HRV along with a tablet being used as the gateway device. The e-ink display can be programmed for warning or suggestive messages.

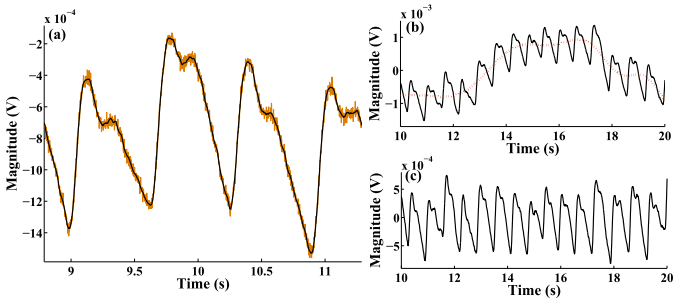

Fig. 8. (a) Comparison between the raw and SG-filtered PPG data. (b) and (c) Illustrating the effect of nonlinear drift removal on preprocessed and detrended PPG. The threshold computed for the illustrated window is 3.8945e-04 V.

from ECG throughout the rest of this paper. This section details the method for detecting the cycle-to-cycle intervals of PPG [PP-interval (PPI)] and the analysis of derived tachogram from PPG and ECG signals. The plot of the cardiac intervals against their instance of occurrence is referred as tachogram. The tachogram for ECG is constructed directly by using the recorded data provided by the eMotion Faros 360°. The cardiac cycle intervals detected from the ECG are referred as RR-intervals (RRIs). To extract the PRV from the collected PPG at wrist, an accurate interval detection technique is critical. Adopted preprocessing techniques play a vital role in determining the accuracy of the detected intervals. These components of the developed algorithm are detailed as follows.

1) Preprocessing Techniques: Mean is removed from the acquired signal to get rid of the inherent offset. Any smoothening or flattening of the signal's peaks or valleys, or any alteration to the signal morphology in the attempt of preprocessing affects the PPI estimation in Section II-C2 and, hence, is inadmissible.

A Savitzky–Golay (SG) filter is used to eliminate the power-line interference and high frequency components if any, during the process of signal acquisition. An SG filter is extensively used for its prominence in preserving the time-domain specific characteristics, like height, shape, and other morphological features of the input waveform. Savitzky and Golay [37] have shown in their work the technique of data smoothening and differentiation using a local least square polynomial fitting. Preservation of sharp transitions is aided by using SG filters. In a simplified version, the technique uses the concept of centering the data around a pivot sample. Then, a specified degree (N) of polynomial is fit to a given window of input data (denoted as $x[n]$), as shown in (1), where b_k refers to the polynomial coefficients

$$g(n) = \sum_{k=0}^{N-1} b_k n^k. \tag{1}$$

Least mean square error (e_n) shown in (2) is used as the optimizing function to evaluate the polynomial coefficients. Formulating the instance of centering the input data about $n = 0$ with a window length of $2M + 1$, the optimizing function is

$$e_n = \sum_{n=-M}^{M} (g(n) - x[n])^2 = \sum_{n=-M}^{M} \left(\sum_{k=0}^{N-1} b_k n^k - x[n] \right)^2. \tag{2}$$

In the given set of normal equations, as shown in (3), for least square approximation to have a unique solution, it is important to have as many data samples as the number of coefficients in the polynomial approximation (N $\leq$ 2M)

$$\sum_{k=0}^{N} \left(\sum_{n=-M}^{M} n^{i+k} \right) b_k = \sum_{n=-M}^{M} n^i x[n] \quad i = 0, 1, 2, \ldots N. \tag{3}$$

Vectorizing (3) to obtain the solutions of the polynomial coefficients shows that it is a simple shift invariant discrete convolution process. The solution is independent of input samples and is dependent only on the order of the polynomial, N, and the window length, $2M + 1$. MATLAB 2016 signal processing tool box is used for realizing an SG filter with a polynomial order of 10 and window length 51 [38]. The equivalent normalized frequency corresponding to the 3-dB cutoff frequency is given as

$$\text{Normalised Frequency} = 2\pi \frac{\text{Cutoff frequency}}{\text{Sampling frequency}}. \tag{4}$$

The choice of polynomial order and window length realize an SG filter, which passes signals with frequency content less than 10 Hz. Fig. 8(a) shows the effect of filtering on the raw waveform collected.

2) PP-Interval Detection Algorithm: For each cycle of the ECG, which is deemed as the truest estimate of a cardiac cycle length, an equivalent pulse cycle is also produced under normal conditions. The estimate of pulse cycle length is carried out based on the boundary conditions applied to the PPG to determine a complete pulse period. In a PPG signal, the steep rising slope owing to the advent of a systolic cycle is referred as an anacrotic phase. It is followed by a catacrotic phase during the diastole. The latter phase encounters a secondary peak owing to the presence of dicrotic notch. In the presented algorithm, the onset of the anacrotic phase is denoted as the pulse foot and is used as the pulse cycle marker. The PPI is the difference between consecutive pulse foots. The algorithm can be divided into two broad sections. First, a search for local

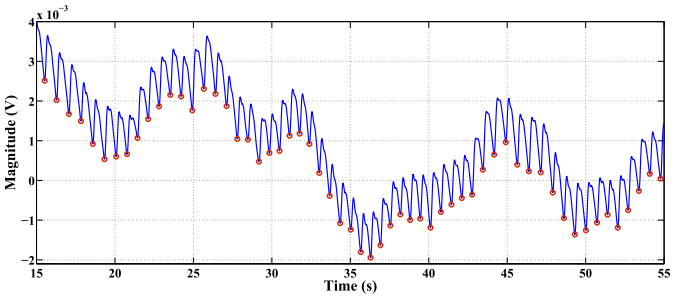

Fig. 9. Pulse foot detection using the adaptive thresholding technique on minimally preprocessed PPG data. This is an illustration of a trimmed segment to show the detection of PPG cycle markers without removing the inherent nonlinear trend.

minima is employed, which is designated as the pulse foot. Second, an adaptive thresholding is incorporated to eliminate the possibility of detecting false peaks. The local minima between two local maxima is designated as pulse foot if it has samples around it higher by a definite threshold. Such a threshold is arrived upon adaptively [39]. The threshold estimation is crucial to avoid detection of the secondary valley encountered during the catacrotic phase in the event of a dicrotic notch.

The following steps are applied to arrive upon a threshold for the concerned window. The final valley-point (pulse foot) detection is carried out utilizing this thresholding criterion on the preprocessed data.

Step 1: The data are trimmed to fixed window length and detrended to remove any linear drift.

Step 2: The statistical least squares technique is used to fit a polynomial to remove any underlying nonlinear tendency. A 20th-order polynomial is evaluated to extract the latent nonlinear component. This derived component is then removed from the data. The graphical depiction of this is shown in Fig. 8(b) and (c).

Step 3: In Steps 1 and 2, the aim is to straighten out the pulse waveform to detect an appropriate threshold. The maximum pulse height obtained is scaled down by one-fourth [40] and assigned as the threshold for the current window. The scaling down is done keeping in mind the usual practical ratio of heights of the pulse peak to the dicrotic notch.

The proposed thresholding eliminates the possibility of detecting the secondary foot encountered during the pulse descent as the pulse foot, as shown in Fig. 9. The fixed window length is taken to be 10 s in this case. It is to be emphasized that Step 2 of the algorithm is applied only to evaluate the threshold. The ultimate pulse foot detection is carried out only on the preprocessed PPG. This information is utilized for the PPI-derived tachogram analysis to derive various HRV indices.

3) Estimation of HRV Indices: Short-term (5 min) HRV's time-domain and frequency-domain parameters are enumerated in Table I [11]. As per the international guidelines [11], duration of 5 min is chosen to allow detection of the lowest frequency component of the LF band (the time period translates to 25 s and at least ten complete cycles are required for a reliable detection). The time-domain variables are calculated by direct implementation of the respective mathematical formulae. The RRIs and PPIs are irregularly spaced owing to the cardiac cycle variability. Hence, the tachograms from ECG and PPG are uniformly sampled at 4 Hz [41] by using cubic spline interpolation prior to spectral estimation. The dc component of tachogram is removed and spectral power is estimated using Welch's averaged periodogram method. Thus, the prominent time- and frequency-domain indices that find significance under diagnostic purposes [42] are evaluated using the proposed wrist-based design in conjunction with the developed algorithm.

TABLE I
DEFINITIONS OF HRV VARIABLES USED IN THIS PAPER

Time domain variables	
NN interval (s)	Cardiac cycle duration (derived from either PPG or ECG)
RMSSD (s)	Root of mean of squared subsequent difference (a common measure of short-term variability)
SDNN (s)	Standard deviation of all NN intervals (a measure of over all variability)
pNN50 (dimensionless)	Ratio of the number of NN intervals more than 50ms and the total number of NN intervals
Frequency domain variables	
LF (normalised unit (n.u))	Low frequencies (0.04-0.15 Hz)
HF (normalised unit (n.u))	High frequencies (0.15-0.40 Hz)
LF/HF (dimensionless)	Ratio of power in respective frequency zones

III. STUDY PROTOCOL

It has been shown that even in healthy individuals, although the variation in ANS in recumbent postures is minimal, there is a clear difference between HRV measurements from supine posture and sitting/standing postures [43]. Given the diagnostic significance of posture maintained during the measurement of HRV, this paper aims to validate the usefulness of the proposed technique under different postural load conditions.

Simultaneous ECG and PPG data were collected using the developed prototype from 20 healthy subjects in three different postures for a duration of 5 min each. Ten male and ten female subjects with an age distribution of 25 $\pm$ 1.8 years (mean $\pm$ standard deviation) and skin tone variation from a scale of I–IV according to Fitzpatrick's classification [44] were included in the study. Subjects without any history of cardiac ailments were chosen for the study. They were asked to refrain from any alcoholic consumption or heavy food ingestion 3 h prior to the study. A written informed consent was obtained from each volunteer, before the commencement of the study. Three postures used in this data collection were supine (T1), pelvic upright while sitting (T2), and standing (T3). The study protocol followed is given in the following.

1) The subject's age and gender are fed into the database before the start of the data collection routine.
2) The subject is allowed to rest in a calm and comfortable room and is familiarized with the equipment.
3) The PPG wrist-based setup is fastened on the nondominant wrist of the subject and the eMotion Faros 360°

ECG monitor is attached with biocompatible electrodes to the subject's chest in the single lead configuration. The subject is confirmed for any case of discomfort before proceeding to record the data.

4) Data are collected in T1 position from the subject for 5 min. The subject is requested to change the posture from T1 to T2.
5) In T2 posture, the subject is asked to sit with crossed legs, upright lower back, and the hands resting on their knees. A habituation time of 2 min is provided, before recording the PPG and ECG signals for a duration of 5 min. The subject is asked to change to posture T3.
6) In T3 posture, the subject is asked to stand with hands dropped down. A span of 2 min is ensured for recovery followed by the 5-min data recording.
7) Subjects are instructed not to indulge in any activity or movement during the period data recording. The subject is asked to relax as much as possible and maintain regular pace of breathing. Data are not recorded during the transition period between the postures.

This study spanned from 20 to 25 min per subject. The subjects were continually checked upon during the entire process for any instance of discomfort.

IV. Experimental Results and Discussion

A. In Vivo Study Results

The designed sensor was initially tested in a wired prototype prior to the development of wrist wearable device. It was compared with the conventional choice of green wavelength (LTT64G, 528 nm) of identical optical specifications as that of yellow–orange wavelength. A study had been conducted on 19 subjects with varied skin tones, in the previous work of the authors and escalated performance of the yellow–orange optical scheme over its counterpart is reported [29]. The skin tone classification was done using the standard Fitzpatrick scale [44]. To ensure the advantage of using longer wavelength, two wearable prototypes were assembled in entirety: one using the optical emitters of 590 nm (LYT64F) and the other of 528 nm (LTT64G). The topology was the same for either wavelength and the pilot study also included the PMMA glass layer. The study was conducted in a consecutive fashion, lest the impact of nondominant or dominant hands alters the results. Also, the pressure applied by the strap was kept constant by ensuring that the wearer uses the same length of the wearable strap in both the devices for a snug fit. The position where the optical sensor comes in contact with the skin is marked to make sure that the same position for each prototype is maintained. A pilot study was conducted on six healthy male individuals falling in the skin tone category of IV by the Fitzpatrick scale. The test settings maintained identically throughout the experiment. For a period of 10 s each, consecutive recordings from the two prototypes of different wavelengths under stationary conditions were carried out. The results of this pilot study are presented in Fig. 10. The signal quality metrics (SQMs) used in [29], signal to noise ratio (SNR), perfusion index (PI), and pulsatile strength show improvement when the longer wavelength is used.

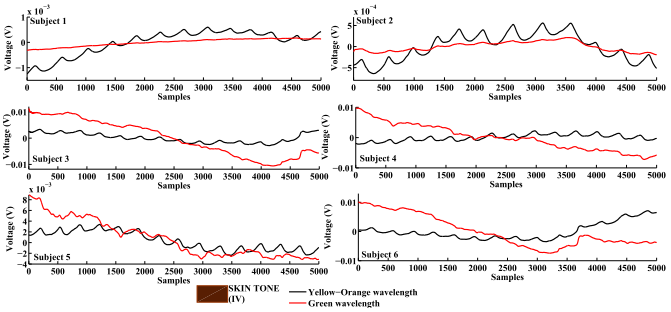

Fig. 10. Illustration of waveforms consecutively collected from six pigmented subjects (skin tone IV) using the developed wearable for longer (590 nm) wavelength and shorter wavelength (520 nm). A swatch corresponding to the skin tone IV is shown as well.

TABLE II
Improvement Factors of the SQMs, Pulsatile Strength, PI, and SNR for a Yellow–Orange (590 nm) Wavelength Over Green (528 nm) Wavelength

Subject ID	Pulsatile Strength	PI	SNR
1*	30.84	67.33	1.60
2	2.48	1.22	2.67
3	2.22	2.80	2.57
4	2.41	1.74	1.31
5	1.26	1.46	2.33
6	3.67	2.09	2.57

*no significant PPG information was contained in the waveform obtained from 528 nm wavelength, hence, the improvement factor is high

The improvement factor for the three indices is defined as the ratio of the SQMs obtained from yellow–orange (590 nm) wavelength to that of green (528 nm) wavelength, as shown in the following:

$$\text{Improvement Factor} = \frac{\text{SQM}_{\text{yellow-orange}}}{\text{SQM}_{\text{green}}}. \tag{5}$$

Table II tabulates the improvement factor attributed to the use of longer wavelength on the three SQMs. The developed device with longer wavelength has a clear advantage over its shorter counterpart in terms of skin pigmentation insensitivity. With a distinctive improvement in the SQMs, the capability of the developed wearable is further investigated for HRV analysis in Sections IV.B and IV.C. Consistent with the previous work of the authors on the use of a longer wavelength optical scheme [29], this developed wrist-based device allows inclusion of wide spectrum of pigmented subjects without any compromise on the quality of detected PPG waveforms.

B. Tachogram Analysis

The tachograms derived from PPG and ECG for a female subject (Subject ID:4) of age 24 in all the three postures for a duration of 5 min have a very high Pearson's correlation (r) between 0.88 and 0.99 ($0.88 < r < 0.99$) for all the described postures. Pearson's correlation is the measure of association between two entities. The closer the absolute value of "r" is to unity, the greater is the association.

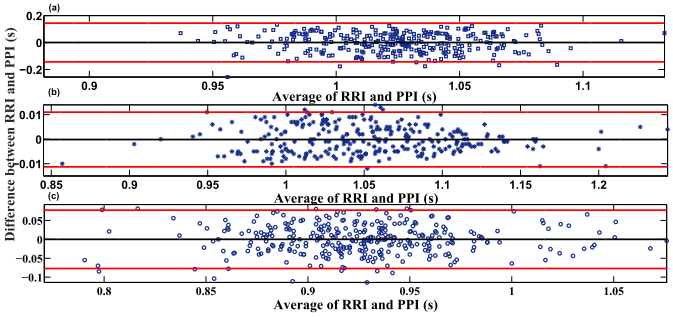

Fig. 11. Bland–Altman showing agreement between the two methods in (a) supine posture with the upper and lower limits of agreement at ±0.1433 BPM, (b) pelvic upright sitting posture with the upper and lower limits of agreement at ±0.0772 BPM, and (c) standing with the upper and lower limits of agreement at ±0.0113 BPM.

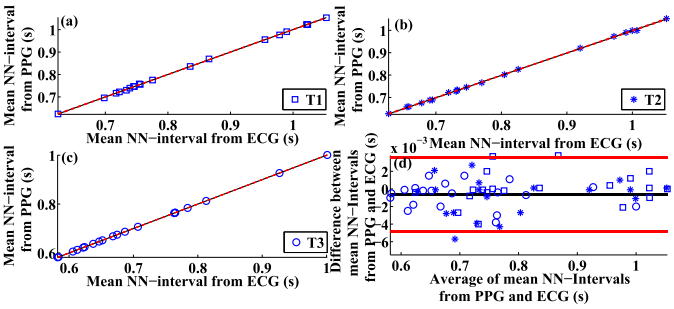

Fig. 12. Average NN-intervals for 5 min for 20 subjects in (a) T1 posture, (b) T2 posture, and (c) T3 posture. (d) Bland–Altman plot of the average NN-intervals for 5 min for 20 subjects in all the postures (the marker annotations for each posture correspond to the previous plots).

The temporal agreement between the two methods is shown using Bland–Altman representation with 95% confidence interval (CI) in Fig. 11(a)–(c) for supine, upright, and standing postures, respectively. Bland–Altman representation involves plotting the error score (difference between the estimates from two methods) on the y-axis and the mean of the estimates from two methods on the x-axis. Accuracy is ensured if the mean error is close to zero and the CIs are tightly grouped around zero. The hypothesized insignificant difference ($\alpha = 5\%$) is backed up with p-values greater than 0.05 ($p > 0.05$) for T1, T2, and T3 in a paired t-test [45] between the two methods for the illustrated subject.

A comparison between the average NN-intervals for all the subjects in the postures T1, T2, and T3 is presented in Fig. 12(a)–(c), respectively. Utilizing the paired t-test, p-values ($p > 0.05$) of 0.095, 0.062, and 0.071 are obtained for T1, T2, and T3, respectively. $p > 0.05$ favors the formulated null hypothesis of insignificant differences between the NN-intervals derived using both approaches. It is also observed that the average NN-interval for a person decreased while progressing from T1 to T3 states. Studies on the effect of posture on heart rate have extensively shown results of increase in heart rate in head-up (vertical) postures in comparison with the horizontal ones [28], [46]–[48]. From Fig. 13, a minimum absolute error in all the subjects can be observed in T1 state. Absolute error in this context is defined

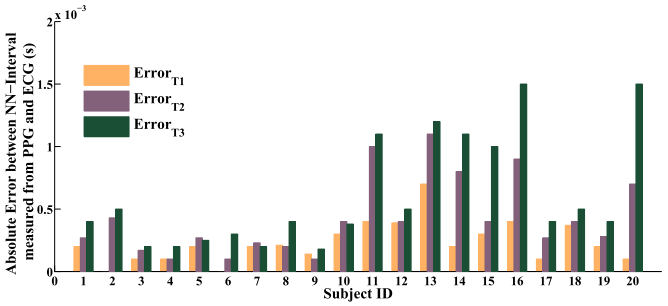

Fig. 13. Absolute error value calculated for $N = 20$ in the estimation of average NN-intervals in all the postures using ECG and PPG-based approaches.

as follows:

$$\text{Absolute Error}_n = |\text{NN Interval}_{\text{ecg}} - \text{NN Interval}_{\text{ppg}}|. \quad (6)$$

However, the trend of increase in the absolute error as we progress from postures T1 to T3 is not monotonous in all the subjects. T3 shows a tendency to have the maximum absolute error in 85% of the cases; in other, it is highly comparable to the absolute error in T2. The average NN-interval derived from all the three postures using the wrist-based PPG agrees with the one derived from ECG as shown in the Bland–Altman plot for all the 60 calculated intervals in Fig. 12(d). The larger absolute error contributed by T3 posture as opposed to T1 posture for the same subject is a result of pronounced effect of additional parameters like gravity at different postural stimulus [49], [50]. Phydro is the hydrostatic pressure produced due to gravity. This is zero in supine posture and increases in recumbent positions. Such effects attribute gravity for change in vascular blood flow rate. This impacts PPG which is a physical (optical in this case) signal when compared with ECG [51] which is an electrical signal. This sensitivity of vascular blood flow to orientation of the measurement site has been shown in many studies [14], [52], [53]. Hence, relative accuracy of PRV in T3 position is less.

C. Analysis of HRV Indices Derived From the Wrist-Based Wearable

The prominent time-invariant time-domain features, root mean square successive difference (RMSSD), standard deviation of NN intervals (SDNN), and mean HR, derived from both the methods are compared for all the subjects using a linear regression model. The details of the fit model, intercept(a_0), and slope(a_1) from the regression analysis for $N = 20$ for all the three postures are provided in Table III. Furthermore, some other metrics of comparison, like root-mean-square error (RMSE), r^2 (a measure of the goodness of the fit model to the real data), and r (Pearson's correlation), are also tabulated in Table III. The minimum values for the average r and r^2 for 20 subjects are 0.948 and 0.892, respectively, corresponding to the T3 posture. Fig. 14(a)–(c) shows the compliance of the wrist-PPG-based approach with ECG to evaluate RMSSD for various postural levels. On running a hypothesis test to evaluate the agreement of RMSSD, with null hypothesis being a zero-point-to-point correlation between the data points,

TABLE III

REPORT OF VARIOUS METRICS OF COMPARISON FOR $N = 20$ IN ALL THE THREE POSTURES FOR HRV PARAMETERS

HRV Feature	Post-ure	A_0	A_1	r	r^2	RMSE
NN-interval	T1	-3.97E-16	1	1	1	1.72E-08
	T2	-0.00027106	0.99873	1	1	0.00268
	T3	-0.0017934	1.0022	1	1	0.00191
RMSSD	T1	0.0034615	0.96135	0.99	0.983	0.00334
	T2	0.0019971	0.97683	0.994	0.987	0.00231
	T3	0.0014856	0.99756	0.968	0.937	0.00227
SDNN	T1	0.00090648	1.0025	0.996	0.992	0.00139
	T2	0.0012697	0.97842	0.982	0.964	0.00235
	T3	0.00096288	0.98008	0.968	0.892	0.00275
LF/HF	T1	-0.015898	1.0207	0.996	0.991	0.0782
	T2	0.00018128	0.95102	0.982	0.981	0.0684
	T3	-0.013896	1.0501	0.948	0.892	0.138

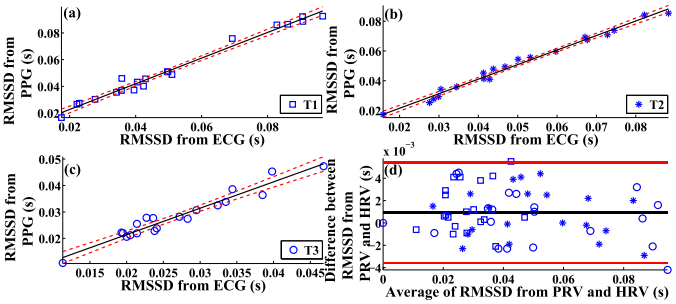

Fig. 14. Average RMSSD for 5 min for 20 subjects in (a) T1 posture, (b) T2 posture, and (c) T3 posture. (d) Bland–Altman plot of the average RMSSD for 5 min for 20 subjects in T1, T2, and T3 postures (the marker annotations for each posture correspond to the previous plots).

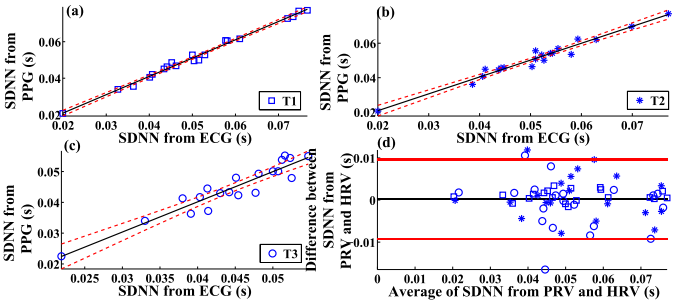

Fig. 15. Average SDNN for 5 min for 20 subjects in (a) T1 posture, (b) T2 posture, and (c) T3 posture. (d) Bland–Altman plot of the average SDNN for 5 min for 20 subjects in T1, T2, and T3 postures (the marker annotations for each posture correspond to the previous plots).

a $p-$value < 0.001 is obtained for all the three postures. This null correlation hypothesis is carried out using two-sided significance limits with Fisher's Z method [54]. The limits of CI of T1 state are the least of all the postures owing to minimum interdata (measures from the two methods) standard error, which is used to compute the coefficients of the two-sided 95% CI. The effect on the estimation of SDNN using the two approaches is shown in Fig. 15. The evaluated RMSE shows an increasing value through the posture T1 followed by T2 and then T3, as tabulated in Table III. Also, in this case, T1 is associated with a tighter confidence band in relation to T2 and T3. However, all the three postures show significant point-to-point correlation between the methods with a p-value less than 0.0001 ($p < 0.0001$). All the three postures

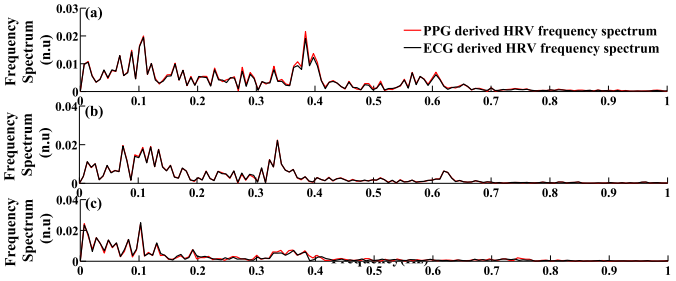

Fig. 16. Frequency spectrum of the RRI and PPI tachograms in (a) T1, (b) T2, and (c) T3 postures.

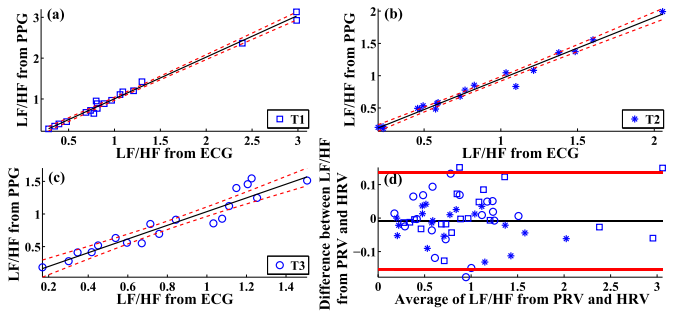

Fig. 17. LF/HF ratio for 5 min for 20 subjects in (a) T1, (b) T2, and (c) T3 postures. (d) Bland–Altman plot of the LF/HF ratio for 5 min for 20 subjects in T1, T2, and T3 postures (the marker annotations for each posture correspond to the previous plots).

have comparable RMSE and show agreeable relation with the confidence bands for the illustrated time-domain HRV features. Also, pNN50 shows $r > 0.985$ for all the three postures, and qualifies the paired t-test with $p > 0.05$ and the point-to-point zero correlation hypothesis with $p < 0.001$.

The accepted frequency-domain features are extracted from the spectrum of the RRI and PPI tachograms [55]. Average power in each band is calculated and the ratio (LF/HF), which is a well-known sympathovagal balance indicator, is assessed using the two approaches. The trend followed in LF/HF value subject to different orthostatic loads is not profound as it also depends on many other aided factors (e.g., breathing rate in the three postures) [56], [57]. Since the objective is to justify the compliance of the developed design for a wrist-based PPG sensor in conjunction with the algorithm as a surrogate to the standard HRV measurement technique (under stationary conditions), we restrict our analysis to the agreement between the spectral features derived from both the methods. An instance of the frequency spectra for a male subject (Subject ID: 14) in all the postures is shown in Fig. 16. The LF/HF shows an appreciable agreement with the t-test ($p > 0.05$) and the null correlation hypothesis ($p < 0.001$). CI is narrower again in case of T1. The RMSE of T3 is higher than that of T1 and T2, which share a relatively comparable RMSE, as shown in Fig. 17(a)–(c). Also, spatial correlation between the defined frequency spectra shows $r > 0.9$ for all the subjects in all the postures. However, in all the three postures, good agreement is justified between the two methods within 95% CI, as shown in the Bland–Altman plots for RMSSD in Fig. 14(d), SDNN in Fig. 15(d), and LF/HF ratio in Fig. 17(d).

V. Conclusion

A wrist-based reflective PPG approach to use PRV as a surrogate to the HRV derived from ECG for the short-term analysis under stationary conditions is presented in this paper. The optical wrist wearable developed uses a novel sensor design with relatively longer wavelength (yellow–orange, 590 nm) optical emitters with dome lens. This allows the inclusion of a wide spectrum of pigmented subjects. A spread out topology in the optical design is used to allow large area of illumination for maximal signal admission. Since the quality of raw signal acquired is important to avoid much preprocessing in the later stage, hardware design is of paramount importance here. Minimal preprocessing was employed prior to the adaptive thresholding valley-detection algorithm for extracting the tachogram from PPG. The agreement of this approach is verified using the standard ECG signal.

Postures and variations in orthostatic load impact the ANS and hence, the interbeat variability. Different postural stimuli hold diagnostic and clinical significance, and hence, validation of the proposed method is carried out under three postural load conditions. The results show statistically insignificant differences between the features derived from PRV and HRV. Supine position can be considered a preferential posture of measurement while using PRV, as it consistently showed the least deviation from the standard reference relative to the other postures in most of the extracted features. Such an observation of increase in deviation from the standard reference, with a progression in postural loads (supine/pelvic upright/standing), can be attributed to the effects of sympathovagal imbalance in the ANS, pronounced effect of gravity on PPG (being a physical signal, contrary to ECG being an electrical one), and dependence of the morphology of PPG on orientation of the measurement site. However, in all the three described postural load conditions, PRV was able to replicate the indices derived from HRV within 95% of CI. Thus, the developed wearable in conjunction with the algorithm is capable of extracting reliable short-term HRV indices from PPG under stationary conditions with various postural load conditions.

References

[1] P. C. Ivanov *et al.*, "Multifractality in human heartbeat dynamics," *Nature*, vol. 399, no. 6735, pp. 461–465, 1999.

[2] R. E. Kleiger, J. P. Miller, J. T. Bigger, Jr., and A. J. Moss, "Decreased heart rate variability and its association with increased mortality after acute myocardial infarction," *Amer. J. Cardiol.*, vol. 59, no. 4, pp. 256–262, 1987.

[3] H. Tsuji *et al.*, "Impact of reduced heart rate variability on risk for cardiac events," *Circulation*, vol. 94, no. 11, pp. 2850–2855, 1996.

[4] D. Bonaduce *et al.*, "Independent and incremental prognostic value of heart rate variability in patients with chronic heart failure," *Amer. Heart J.*, vol. 138, no. 2, pp. 273–284, 1999.

[5] H. Mølgaard, K. E. Sørensen, and P. Bjerregaard, "Attenuated 24-h heart rate variability in apparently healthy subjects, subsequently suffering sudden cardiac death," *Clin. Auto. Res.*, vol. 1, no. 3, pp. 233–237, 1991.

[6] G. A. R. del Paso, W. Langewitz, L. J. Mulder, A. van Roon, and S. Duschek, "The utility of low frequency heart rate variability as an index of sympathetic cardiac tone: A review with emphasis on a reanalysis of previous studies," *Psychophysiology*, vol. 50, no. 5, pp. 477–487, 2013.

[7] N. Hjortskov, D. Rissén, A. K. Blangsted, N. Fallentin, U. Lundberg, and K. Søgaard, "The effect of mental stress on heart rate variability and blood pressure during computer work," *Eur. J. Appl. Physiol.*, vol. 92, nos. 1–2, pp. 84–89, 2004.

[8] B. Pomeranz *et al.*, "Assessment of autonomic function in humans by heart rate spectral analysis," *Amer. J. Physiol.-Heart Circulatory Physiol.*, vol. 248, no. 1, pp. H151–H153, 1985.

[9] A. E. Aubert, B. Seps, and F. Beckers, "Heart rate variability in athletes," *Sports Med.*, vol. 33, no. 12, pp. 889–919, 2003.

[10] T. Rechlin, M. Weis, A. Spitzer, and W. P. Kaschka, "Are affective disorders associated with alterations of heart rate variability?" *J. Affective Disorders*, vol. 32, no. 4, pp. 271–275, 1994.

[11] European Society of Cardiology, "Heart rate variability standards of measurement, physiological interpretation, and clinical use," *Eur. Heart J.*, vol. 93, pp. 1043–1065, Mar. 1996.

[12] J. T. Bigger, J. L. Fleiss, L. M. Rolnitzky, and R. C. Steinman, "The ability of several short-term measures of rr variability to predict mortality after myocardial infarction," *Circulation*, vol. 88, no. 3, pp. 927–934, 1993.

[13] K. B. Min, J.-Y. Min, D. Paek, S.-I. Cho, and M. Son, "Is 5-minute heart rate variability a useful measure for monitoring the autonomic nervous system of workers?" *Int. Heart J.*, vol. 49, no. 2, pp. 175–181, 2008.

[14] T. Tamura, Y. Maeda, M. Sekine, and M. Yoshida, "Wearable photoplethysmographic sensors—Past and present," *Electronics*, vol. 3, no. 2, pp. 282–302, 2014.

[15] M. Nitzan, A. Babchenko, B. Khanokh, and D. Landau, "The variability of the photoplethysmographic signal—A potential method for the evaluation of the autonomic nervous system," *Physiol. Meas.*, vol. 19, no. 1, p. 93, 1998.

[16] J. Lázaro, E. Gil, J. M. Vergara, and P. Laguna, "Pulse rate variability analysis for discrimination of sleep-apnea-related decreases in the amplitude fluctuations of pulse photoplethysmographic signal in children," *IEEE J. Biomed. Health Inform.*, vol. 18, no. 1, pp. 240–246, Jan. 2014.

[17] G. Lu, F. Yang, J.-A. Taylor, and J.-F. Stein, "A comparison of photoplethysmography and ecg recording to analyse heart rate variability in healthy subjects," *J. Med. Eng. Technol.*, vol. 33, no. 8, pp. 634–641, 2009.

[18] A. Schäfer and J. Vagedes, "How accurate is pulse rate variability as an estimate of heart rate variability?: A review on studies comparing photoplethysmographic technology with an electrocardiogram," *Int. J. Cardiol.*, vol. 166, no. 1, pp. 15–29, 2013.

[19] J. Hayano, A. K. Barros, A. Kamiya, N. Ohte, and F. Yasuma, "Assessment of pulse rate variability by the method of pulse frequency demodulation," *BioMed. Eng. OnLine*, vol. 4, no. 1, p. 62, 2005.

[20] A. Choi and H. Shin, "Photoplethysmography sampling frequency: Pilot assessment of how low can we go to analyze pulse rate variability with reliability?" *Physiol. Meas.*, vol. 38, no. 3, p. 586, 2017.

[21] L. G. G. Porto and L. F. Junqueira, Jr., "Comparison of time-domain short-term heart interval variability analysis using a wrist-worn heart rate monitor and the conventional electrocardiogram," *Pacing Clin. Electrophysiol.*, vol. 32, no. 1, pp. 43–51, 2009.

[22] C.-S. Chu *et al.*, "A finger-free wrist-worn pulse oximeter for the monitoring of chronic obstructive pulmonary disease," *Proc. SPIE*, vol. 9698, p. 96981C, Mar. 2016.

[23] K. V. Madhav, M. R. Ram, E. H. Krishna, N. R. Komalla, and K. A. Reddy, "Robust extraction of respiratory activity from PPG signals using modified MSPCA," *IEEE Trans. Instrum. Meas.*, vol. 62, no. 5, pp. 1094–1106, May 2013.

[24] S. S. Thomas, V. Nathan, C. Zong, K. Soundarapandian, X. Shi, and R. Jafari, "BioWatch: A noninvasive wrist-based blood pressure monitor that incorporates training techniques for posture and subject variability," *IEEE J. Biomed. Health Inform.*, vol. 20, no. 5, pp. 1291–1300, Sep. 2016.

[25] C. Mathias and R. Bannister, *Investigation of Autonomic Disorders*. Oxford, U.K.: Oxford Univ. Press, 1999.

[26] J. C. Mathias, "Autonomic diseases: Clinical features and laboratory evaluation," *J. Neurol., Neurosurgery Psychiatry*, vol. 74, pp. iii31–iii41, Sep. 2003.

[27] M. Gilder and R. Ramsbottom, "Change in heart rate variability following orthostasis relates to volume of exercise in healthy women," *Auto. Neurosci.*, vol. 143, no. 1, pp. 73–76, 2008.

[28] N. Watanabe, J. Reece, and B. I. Polus, "Effects of body position on autonomic regulation of cardiovascular function in young, healthy adults," *Chiropractic Osteopathy*, vol. 15, no. 1, p. 19, 2007.

[29] P. Mohapatra, S. P. Preejith, and M. Sivaprakasam, "A novel sensor for wrist based optical heart rate monitor," in *Proc. IEEE Int. Instrum. Meas. Technol. Conf. (I2MTC)*, Turin, Italy, May 2017, pp. 1–6.
[30] R. R. Anderson and J. A. Parrish, "The optics of human skin," *J. Invest. Dermatol.*, vol. 77, no. 1, pp. 13–19, 1981.
[31] D. T. Delpy and M. Cope, "Quantification in tissue near–infrared spectroscopy," *Philos. Trans. Roy. Soc. London B, Biol. Sci.*, vol. 352, no. 1354, pp. 649–659, 1997.
[32] J. Liu, B. P.-Y. Yan, W.-X. Dai, X.-R. Ding, Y.-T. Zhang, and N. Zhao, "Multi-wavelength photoplethysmography method for skin arterial pulse extraction," *Biomed. Opt. Exp.*, vol. 7, no. 10, pp. 4313–4326, 2016.
[33] Y. Maeda, M. Sekine, T. Tamura, A. Moriya, T. Suzuki, and K. Kameyama, "Comparison of reflected green light and infrared photoplethysmography," in *Proc. 30th Annu. Int. Conf. IEEE Eng. Med. Biol. Soc. (EMBS)*, Aug. 2008, pp. 2270–2272.
[34] A. N. Bashkatov, E. A. Genina, V. I. Kochubey, and V. V. Tuchin, "Optical properties of human skin, subcutaneous and mucous tissues in the wavelength range from 400 to 2000 nm," *J. Phys. D, Appl. Phys.*, vol. 38, no. 15, p. 2543, 2005.
[35] R. M. Ahmed, "Optical study on Poly(methyl methacrylate)/poly (vinyl acetate) blends," *Int. J. Photoenergy*, vol. 2009, Aug. 2009, Art. no. 150389.
[36] C. Orphanidou, T. Bonnici, P. Charlton, D. Clifton, D. Vallance, and L. Tarassenko, "Signal-quality indices for the electrocardiogram and photoplethysmogram: Derivation and applications to wireless monitoring," *IEEE J. Biomed. Health Inform.*, vol. 19, no. 3, pp. 832–838, May 2015.
[37] A. Savitzky and M. J. E. Golay, "Smoothing and differentiation of data by simplified least squares procedures," *Anal. Chem.*, vol. 36, no. 8, pp. 1627–1639, 1964.
[38] C. Zuo, Q. Chen, Y. Yu, and A. Asundi, "Transport-of-intensity phase imaging using savitzky-golay differentiation filter—Theory and applications," *Opt. Exp.*, vol. 21, no. 5, pp. 5346–5362, 2013.
[39] E. Billauer. (2008). *peakdet: Peak Detection Using MATLAB*. [Online]. Available: http://billauer.co.il/peakdet.html
[40] X. Wang, W. Wang, X. Lu, and P. Zhou, "Pulse wave detection for ultrasound imaging," in *Recent Advances in Computer Science and Information Engineering*. Berlin, Germany: Springer, 2012, pp. 633–638.
[41] J.-P. Niskanen, M. P. Tarvainen, P. O. Ranta-Aho, and P. A. Karjalainen, "Software for advanced HRV analysis," *Comput. Methods Programs Biomed.*, vol. 76, no. 1, pp. 73–81, 2004.
[42] L. Hejjel and I. Gal, "Heart rate variability analysis," *Acta Physiol. Hungarica*, vol. 88, nos. 3–4, pp. 219–230, 2001.
[43] A. D. Ryan, P. D. Larsen, and D. C. Galletly, "Comparison of heart rate variability in supine, and left and right lateral positions," *Anaesthesia*, vol. 58, no. 5, pp. 432–436, 2003.
[44] S. Sachdeva *et al.*, "Fitzpatrick skin typing: Applications in dermatology," *Indian J. Dermatol., Venereol., Leprol.*, vol. 75, no. 1, p. 93, 2009.
[45] R. Zaki, A. Bulgiba, R. Ismail, and N. A. Ismail, "Statistical methods used to test for agreement of medical instruments measuring continuous variables in method comparison studies: A systematic review," *PLoS ONE*, vol. 7, no. 5, p. e37908, 2012.
[46] J. A. MacWilliam, "Postural effects on heart-rate and blood-pressure," *Quart. J. Experim. Physiol.*, vol. 23, no. 1, pp. 1–33, 1933.
[47] A. Y. M. Jones *et al.*, "Changes in heart rate and R-wave amplitude with posture," *Chin. J. Physiol.*, vol. 46, no. 2, pp. 63–70, 2003.
[48] M. Choe *et al.*, "Effect of changing position from supine to standing up-right on the circulation in young men and women," *J. Nurses Acad. Soc.*, vol. 19, no. 3, pp. 285–298, 1989.
[49] A. Grollman, "The effect of variation in posture on the output of the human heart," *Amer. J. Physiol.-Legacy Content*, vol. 86, no. 2, pp. 285–301, 1928.
[50] M. Rohdin *et al.*, "Effects of gravity on lung diffusing capacity and cardiac output in prone and supine humans," *J. Appl. Physiol.*, vol. 95, no. 1, pp. 3–10, 2003.
[51] J. E. Madias, "Comparability of the standing and supine standard electrocardiograms and standing sitting and supine stress electrocardiograms," *J. Electrocardiol.*, vol. 39, no. 2, pp. 142–149, 2006.
[52] S.-Z. Xin *et al.*, "Investigation of blood pulse ppg signal regulation on toe effect of body posture and lower limb height," *J. Zhejiang Univ.-Sci. A*, vol. 8, no. 6, pp. 916–920, 2007.
[53] J. Muehlsteff, X. A. Aubert, and G. Morren, "Continuous cuff-less blood pressure monitoring based on the pulse arrival time approach: The impact of posture," in *Proc. 30th Annu. Int. Conf. IEEE Eng. Med. Biol. Soc.*, Aug. 2008, pp. 1691–1694.
[54] M. C. Whitlock, "Combining probability from independent tests: The weighted Z-method is superior to Fisher's approach," *J. Evol. Biol.*, vol. 18, no. 5, pp. 1368–1373, 2005.
[55] D. L. Eckberg, "Sympathovagal balance," *Circulation*, vol. 96, no. 9, pp. 3224–3232, 1997.
[56] M. Bootsma, C. A. Swenne, M. J. A. Janssen, V. M. Cats, and M. J. Schalij, "Heart rate variability and sympathovagal balance: Pharmacological validation," *Netherlands Heart J.*, vol. 11, no. 6, pp. 250–258, 2003.
[57] J. J. Goldberger, "Sympathovagal balance: How should we measure it?" *Amer. J. Physiol.-Heart Circulatory Physiol.*, vol. 45, no. 4, pp. H1273–H1280, 1999.

Payal Mohapatra received the M.S. degree (by research) in electronics and instrumentation engineering from the Madras Institute of Technology, Chennai, India, in 2015.

She is currently a Graduate Student with the Department of Electrical Engineering, IIT Madras, Chennai. Her current research interests include cardiological healthcare devices in wearable technology and signal processing for biomedical applications.

Preejith Sreeletha Premkumar received the bachelor's degree in electronics and communication from the Sree Chitra Thirunal College of Engineering, Thiruvananthapuram, India, in 2011, and the M.S. degree in electrical engineering from IIT Madras, Chennai, India, in 2013.

He is currently the System Designer with the Healthcare Technology Innovation Centre, IIT Madras, and deals with hardware projects involving sensors and instrumentation, with the primary focus on wearable devices for clinical applications. His current research interests include minimally intrusive physiological monitoring, biomechanics, and endoscopy.

Mohanasankar Sivaprakasam after the Ph.D. and Post-Doctoral Research in the U.S. in implantable medical devices for eight years, he returned to India with a goal of developing affordable medical technologies in the country. Since 2009, he has been successfully developing an ecosystem of technologists, clinicians and industry, culminating in setting up of Healthcare Technology Innovation Centre (HTIC), IIT Madras, Chennai, India, in 2011, where he is currently with the Faculty of Electrical Engineering, and the Director of HTIC. He has authored over 80 peer-reviewed publications in journals and conferences.